Moroccan Journal of Chemistry
ISSN: 2351-812X

Mor. J. Chem., 2023, Volume 11, Issue 02, Page 350-360
https://revues.imist.ma/index.php/morjchem
https://doi.org/10.48317/IMIST.PRSM/morjchem-xxxx-xxxx

Synthesis and characterization of Mn/Ce-Doped TiO_2: Investigation of structural and optical properties

Zobair Elafia[1,2*], Mohamed Youssef Messous[3], Belkheir Hammouti[4], Mohamed Cherkaoui[1]

[1]*Laboratory of Organic Chemistry, Catalysis and Environment, Faculty of Sciences, University Ibn Tofail, Kenitra, Morocco.*
[2]*National Center for Energy, Sciences and Nuclear Techniques CNESTEN, Radiometric Unit Rabat, Morocco*
[3]*National Center for Energy, Sciences and Nuclear Techniques CNESTEN, Material Sciences Unit (USM/DERS), Rabat, Morocco*
[4]*Laboratory of Industrial Engineering, Energy and the Environment (LI3E), SupMTI, Rabat, Morocco*

**Corresponding author, Email address: zobair.elafia@gmail.com*

Received *02 Jan 2023,*
Revised *20 Feb 2023,*
Accepted *22 Feb 2023*

Citation*: Elafia Z., Messous Y.M., Hammouti B., Cherkaoui M. (2023 Synthesis and characterization of Mn/Ce-Doped TiO_2: Investigation of structural and optical properties, Mor. J. Chem., 14(2), 350-359. Doi: https://doi.org/10.48317/IMIST.PRSM/morjchem-v11i2.35078*

Abstract: The improvement of the optical properties of Titanium dioxide by doping with transition metals and rare earth ions is one of the most studies carried out by researchers. In this paper the TiO_2: 0,01 Mn^{2+} x Ce^{3+} (x= 0; 1; 2 and 5 mol%) was synthesized by co-precipitation way. The structural and morphological properties were defined using X-ray diffraction, Fourier Transformation Total Infrared Reflection (FTIR), Raman Spectroscopy and Scanning Electron Microscopy coupled with Energy Dispersive X-ray (SEM/EDX). The optical properties have been studied by UV-Visible spectroscopy. The co-doping with Ce^{3+} affects the lattice parameters of TiO_2 and decreases the optical gap energy E_g which improve the absorption capability in the UV-Visible region. The results are discussed.

Keywords: Optical properties; Titanium dioxide; co-precipitation; Scherrer method; Williamson-hall method; structural properties.

Introduction

Titanium dioxide TiO_2 is a broadband non-toxic semiconductor with high chemical stability, thermal stability and photocatalytic efficiency (Juhana *et al.* 2022, Kanan *et al.*, 2020, Komaraiaha *et al.*, 2019). TiO_2 exists in nature as three polymorphs viz rutile, anatase and brookite. The rutile is the most crystal prevalent form of titanium dioxide (Karishma *et al.* 2020, Cho *et al.*, 2022). The band gap energy is approximately 3.02 eV for rutile and 3.2 eV for anatase, this wide band gap gives TiO_2 the ability to absorb the ultraviolet (UV) light where, the wavelength is less than 380 nm (Ilie *et al.*, 2017; Nasir *et al.*, 2014). TiO_2 has attracted the attention of researchers seen his unique proprieties and his wide applications area in the optic devices, the lasers of solid state, telecommunications systems, biosensors

and especially in the photovoltaic solar cells (Salhi *et al.*, 2016). Several techniques are used for the synthesis of TiO_2 as hot dip deposition centrifugal, sol gel coating with filtered arc and co-precipitation (Roman *et al.* 2017, Luiz *et al.*, 2021, Winfred *et al.* 2016, Ghulam *et al. 2020, Asept et al.2022*). Spectroscopies techniques are essential means for the characterization of nanoparticles in many laboratories due to the sensitive interconnection between the vibrational behavior and the structure, composition and properties of the material. The modification of the structural properties of the material induced a shift, an increase in size, an electron-phonon coupling, combinations and harmonics of the vibrational spectra compared to the bulk material (Aguilar *et al.* 2019). In this study, the main goal is the improvement of optical proprieties of TiO_2. In order to have better results doping TiO_2 is a good option by using various transition metals such as Cd, V, Cr, Mo, Zn, Co, and specially Mn, these metallic elements trap electrons and holes to reduce electron hole recombination rates. As the Manganese and the Titanium have similar sizes, the two elements incorporate very well together in order to get better charge mobility. Therefore, using Manganese help altering the intrinsic optoelectronic properties, and by creating defect sites on the d-band states it can reduce the wide band gap of the TiO_2 and improve the absorption of the visible light and refine the optical properties to high oxygen mobility (Milan *et al.* 2020, Devi *et al.*, 2020, Kaur *et al.*, 2017, Siyoung *et al.*, 2022).Since Mn^{2+} known by its poor emission efficiency due to the spin-forbidden $^4T_1(4G)/^6A_1(6S)$ transition, an additional ion needed to be used to promote the Mn^{2+} excitation and improve the emission intensity, for this matter the Ce^{3+} provide the best intended results as its 5d–4f transitions act as an activator in Titanium TiO_2 to emit broadband visible light (Liao *et al.*, 2020).

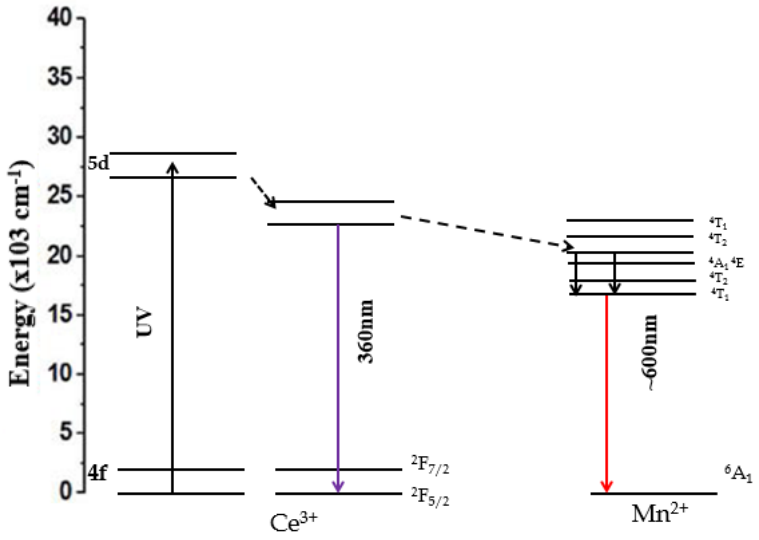

Figure 1. Schematic level diagram for Energy transfer between Ce^{3+} and $Mn^{2+}$for photonic conversion.

The energy level diagram presented in **Figure 1** shows the energy transfer process between the excited levels of Ce^{3+} and Mn^{2+}.With the energy difference between Ce^{3+} and Mn^{2+} the possibility of the energy transfer occurs within the non-radiative transitions from the lowest 5d excited of Ce^{3+} to the $^4T_2$ level of Mn^{2+}ion by assistance of phonons. Under the UV-light radiation the Ce^{3+} electrons raise to higher component of 5d level then relaxes to the 5d crystal field splitting state, and then it regress to the $^2F_{5/2}$ and $^2F_{7/2}$ spin-orbit split 4f ground state by releasing photons with similar values of the energy levels, an energy transfer happens from the excited 5d state of the Ce^{3+} to $^4T_2$ level of Mn^{2+}, this manganese ion level relaxes to the $^4T_1$ level and then decompose nonradiatively to the $^6A_1$ ground state that improve the Mn^{2+} emission properties mobility (Junrong *et al.* 2020, Susana *et al.*, 2016).

2. Methodology

2.1 Materials and instruments

Titanium (III) chloride $TiCl_3$ (purity ≥ 99.95%) purchased from Sigma Aldrich is used for un-doped TiO_2 preparation. The precursors $MnCl_2{\cdot}4H_2O$ (98%), $CeCl_3{\cdot}7H_2O$ (99.9%) received also from Sigma Aldrich are used as Mn and Ce source respectively for doping TiO_2.The un-doped and Ce/Mn doped TiO_2 were characterized by Attenuated Total Reflection-Fourier Transform Infrared ATR-FTIR (Perkin-Elmet spectrometer UATR two), X-Ray diffraction XRD (D2-PhaserDiffractometer from Bruker), Raman spectroscopy (Renishaw 1000 B spectrometer),diffuse reflectance spectroscopy UV-Vis and scanning electron microscopy SEM (Quanta 200).

2.2 Experiments

For the synthesis of TiO_2 doped with Mn (TCM0), a volume of 5 mL of titanium tri-chloride ($TiCl_3$) solution was mixed with 40 mL of di-ionized water and a portion of 10% of Mn in an Erlenmeyer flask. The pH of the solution was then adjusted by adding a few drops of ammonium hydroxide NH_4OH. The mixture was placed on a magnetic stirrer heated at 60° C with continuous stirring for 3 hours. The solution is left for settling for 24 hours. The precipitate was filtered with 0.45 µm porosity filter, the filtra is then dried in an oven at 105 °C for 24 hours. For the preparation of the samples (TCM1, TCM2 and TCM3) amounts of $MnCl_2{\cdot}4H_2O$ and $CeCl_3{\cdot}7H_2O$ were added according to the stoichiometries 10% of Manganese and 1%, 2% and 5% with the same protocol.

3. Results and Discussion

3.1 X-Ray Diffraction Analysis (XRD)

Figure 2 shows the XRD patterns of Mn-doped and Ce/Mn co-doped TiO_2. For Mn-doped TiO_2 (TCM0) the rutile phase is indicated by the presence of an exhibited diffraction peaks shows at 2θ=27.26°; 35.97°; 54.19°; 41.2°; 56.41° and 69.75° (Haque *et al.* 2017, Li *et al.*, 2014, Boxiong *et al.*, 2010, El Afia et al.2020). Whereas the peaks at 25.07° (101) and 62.69° corresponding to the anatase phase (Zengping *et al.* 2016). For The others sample Mn/Ce doped TiO_2 (TCM1, TCM2 and TCM3) the spectrum shows the presence of the same peaks corresponding to anatase and rutile crystalline phases with a slight shifting. The spectrum shows that all samples have almost identical peak positions with absence of diffraction patterns associated with compounds derived from Manganese and Cerium. This absence may be due to the incorporation of Mn and Ce into TiO_2 lattice, or these species were very dispersed on the surface of TiO_2, or presumably due to the low concentration of the Mn and Ce dopants. The crystal size D of TiO_2 was estimated by using Scherrer **Eqn. 1** and Williamson-Hall method **Eqn.2** (Mustapha *et al.* 2021, Kibasomba *et al.*, 2018). The concept of this method is plotting the curve βcosθ versus 4sinθ (figure 4), the interception of this graph is (Kλ)/D. Using y = (Kλ)/D, the crystallite size is calculated from D = (Kλ)/y and the slope deduced from the curve presented the strain (ε):

$$D = \frac{K\lambda}{\beta \cos\theta} \qquad \textbf{Eqn. 1}$$

$$\beta\cos\theta = \frac{K\lambda}{D} + 4.\varepsilon.sin\theta \qquad \textbf{Eqn. 2}$$

Where λ is the wavelength incident X-ray (= 1.549 Å); K isshape factor (= 0.9); β is Full-width at half maximum (FWHM) of the peak in the XRD patterns and θ is diffraction angle. ε is the strain.

Table 1 illustrates the crystals size D, the stain (ε) and the lattice parameters of all samples. The average crystallites size of TiO_2 calculated by the two Scherrer and Williamson - Hall methods are much closed as indicated in **figure 3**. The results show that doping with Mn and Ce ions infect the crystal size and strains lattice of TiO_2 (Xiaojun *et al.* 2017, Meddouri *et al.*, 2016). The results are presented in table 1 and they consistent with literature (Zhang *et al.* 2016):

Table 1. lattice parameters of Mn/Ce doped TiO_2

	$D_{sherrer}$ (nm)	D_{W-H} (nm)	a (nm)	c (nm)	V(Å^3)	ε(%)
TCM_0	13.2	29	5.3	2.5	62.53	$-2.6.10^{-3}$
TCM_1	8.8	11.9	5.3	2.5	63.01	10^{-3}
TCM_2	15.88	10.48	5.3	2.5	62.14	$-2.9.10^{-3}$
TCM_3	18.13	10.48	5.3	2.5	62.33	$-2.9.10^{-3}$

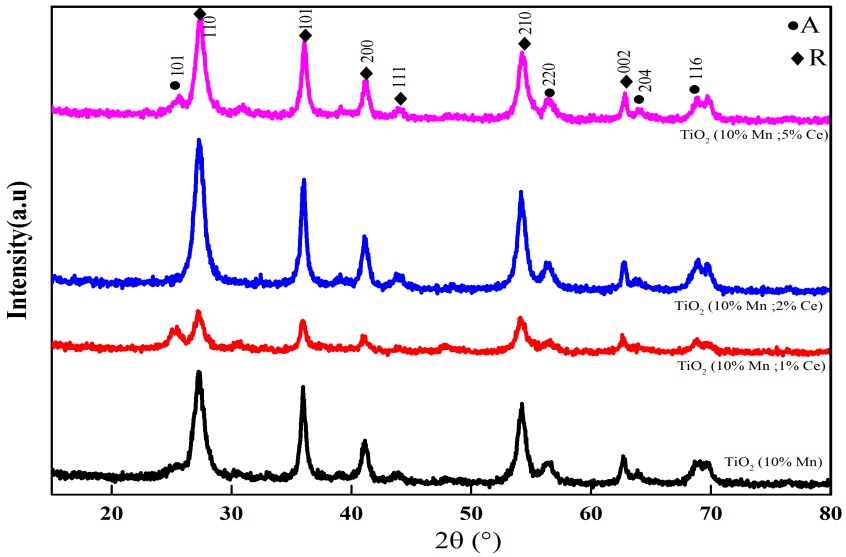

Figure 1. XRD patern of Mn doped and Mn/Ce co-doped TiO_2

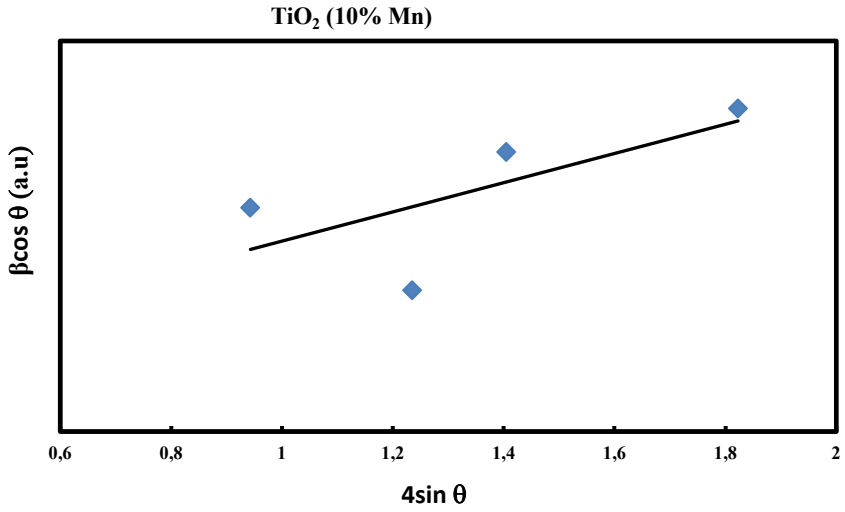

Figure 3. Graphical presentation of β.cosθ versus 4.sinθ of Mn doped TiO_2

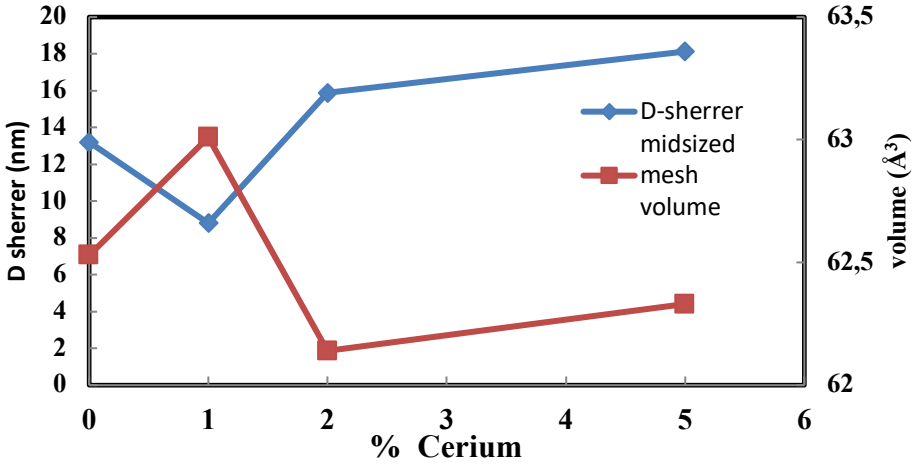

Figure 4. Graphical presentation of Size sheerer and Volume (V) of Mn/Ce doped TiO_2.

3.2 Fourier Transform Infrared Spectroscopy (ATR-FTIR)

The Fourier transform infrared spectroscopy (FTIR)was used to define the functional groups present in the synthesized material. The **figure 5** showed the FTIR spectra for Mn doped TiO_2 and Mn/Ce co-doped TiO_2, strong bands have been seen at the region 530,47 cm^{-1} and 629,42 cm^{-1} corresponding respectively to Mn-O-Ti and O-Ti-O vibrational mode (Al-Amin *et al.* 2016). These results were in agreement with earlier reported studies. Stretching and bending vibration of hydroxyl groups of all loaded materials were in the range of 3200–3600 cm^{-1} and 1617–1635 cm^{-1} (Zahid *et al.* 2018). All The FTIR results confirm the formation of TiO_2 nanomaterial.

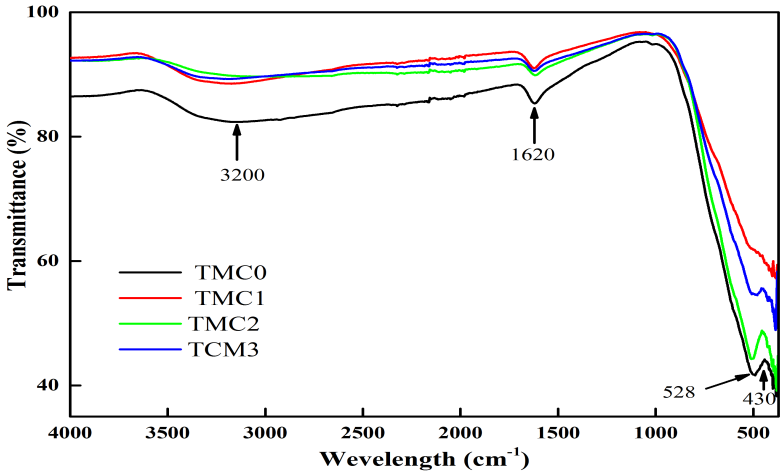

Figure 5. FTIR spectra of Mn doped TiO_2 and Mn/Ceco-doped TiO_2

3.3 Shift Raman

Figure 6 shows the Raman spectra of synthesized TiO_2 doped with manganese and cerium. Raman peaks are sensitive to any change occurring in theTiO_2 lattice when dopant is added into the interstitial site. The insertion of Mn^{2+}distorts the TiO_2 lattice, or a strain is induced by a decrease in the number of oxygen atoms bonded with Ti (Sharotri *et al.* 2019). The spectrum showed a rutile mode at E_g around

437 cm^{-1} ,while for anatase phase the modes are B_{1g}~357 cm^{-1},A_{1g} + B_{1g} ~ 516 $cm^{-1}$and E_g ~ 600 cm^{-1} (Scarisoreanu *et al.* 2019).

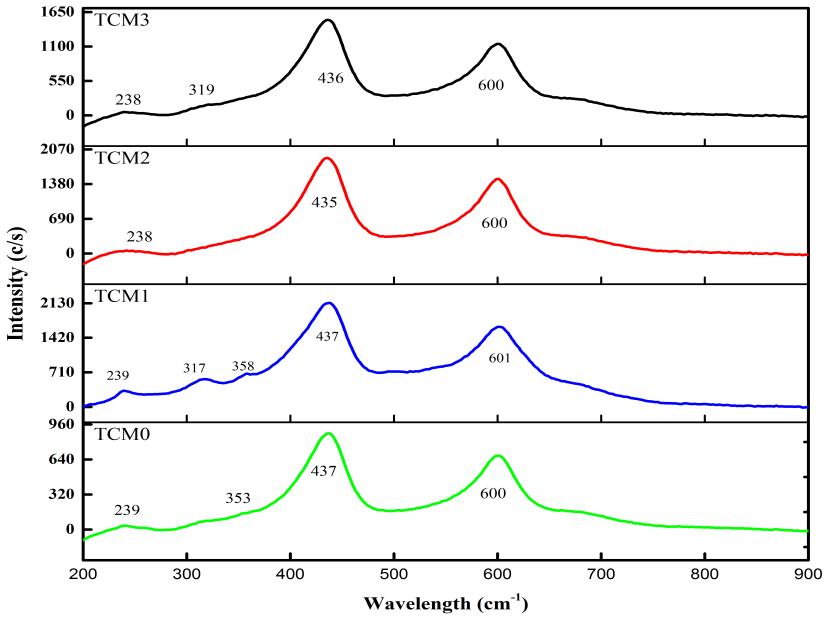

Figure 6. Raman shift spectra of synthesized TiO_2 doped on Mn and Ce TCM_0 ; TCM_1; TCM_2 and TCM_3

3.4 SEM Spectroscopy

The surface morphology of the prepared titanium dioxide samples studied by using scanning electron microscope (SEM). **Figure 7** (a; b) shows respectively the SEM image (10 µm scale) of doped by manganese and co-doped by manganese and Cerium. It's remarkable that the samples are regular in shape and there is no significant change in the morphology of the surface after doping with Cerium.

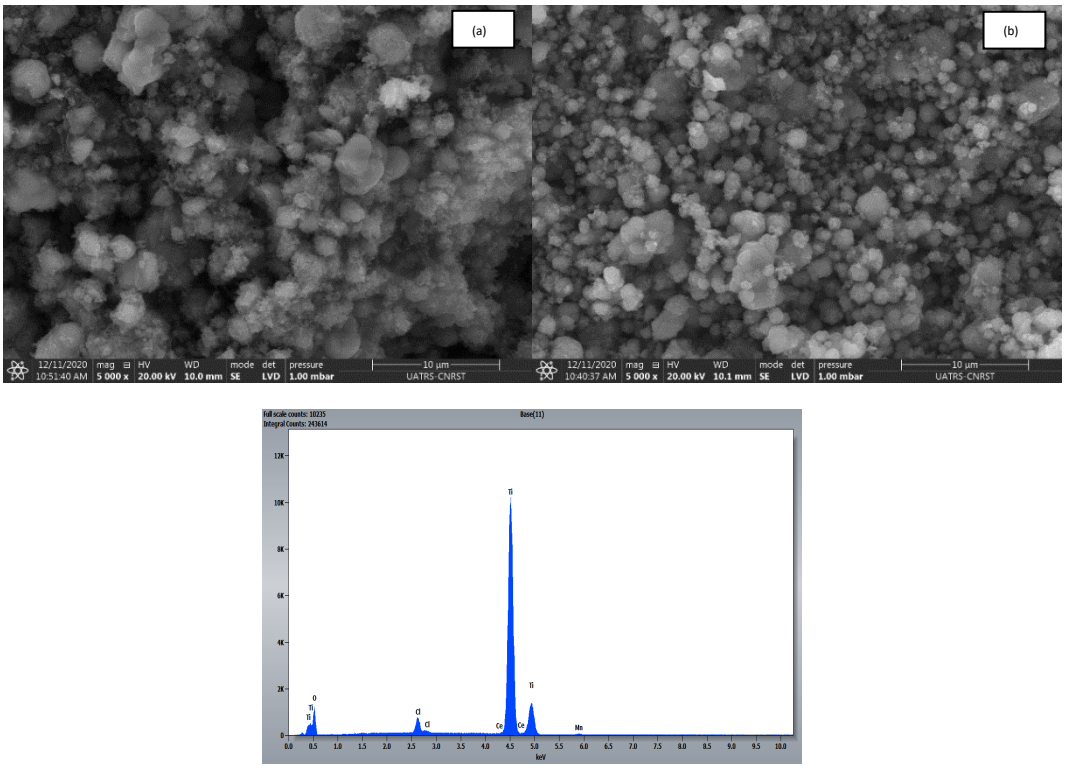

Figure 7. SEM images of Mn Doped TiO_2 TCM_0(b); Mn/Ce doped TiO_2 TCM_3 (c) & EDX spectrum of TCM3

3.5 UV–Vis Absorption

The **figure 8** presents the UV-Visible absorption spectrum of Mn-TiO_2 and Mn/Ce co-doped TiO_2 curried out from 200 to 1000 nm at room temperature. The spectrums show a height intensity absorption band in UV region around 320 nm corresponding to the charge transfer between Oxygen and titanium atoms. The absorption was enhanced due to the incorporating Mn and Ce dopants into the TiO_2 lattice.

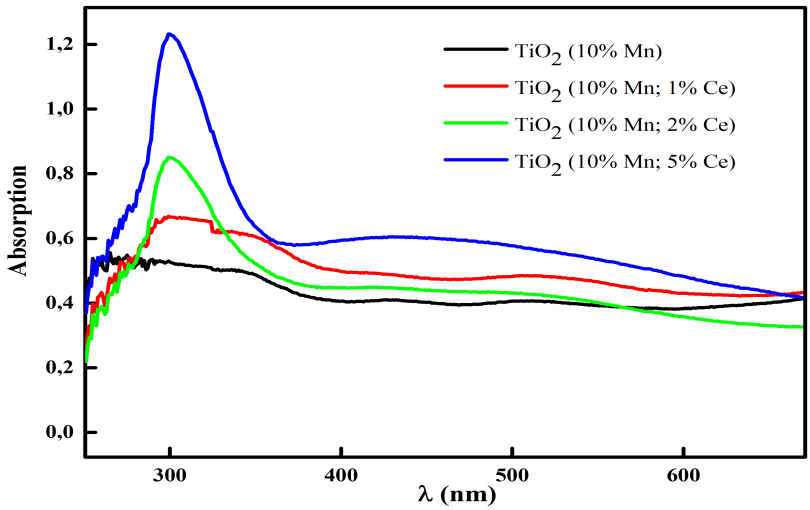

Figure 8. UV-Visible spectra of Mn/Ce doped TiO_2

The optical gap of TiO_2 was determined using the Tauc method **Eqn. 3** (Li, *et al.* 2014), this method is based by plotting energy (Eg) and the optical absorption coefficient **figure 9**. The band gap decreased which improved its absorption efficiency (Tbessi *et al.* 2018).

$$\alpha h\upsilon = B(h\upsilon - Eg)^{\frac{1}{2}} \quad \textbf{Eqn. 3}$$

Where B is proportionality constant and $h\upsilon$ is the energy of the incident photon.

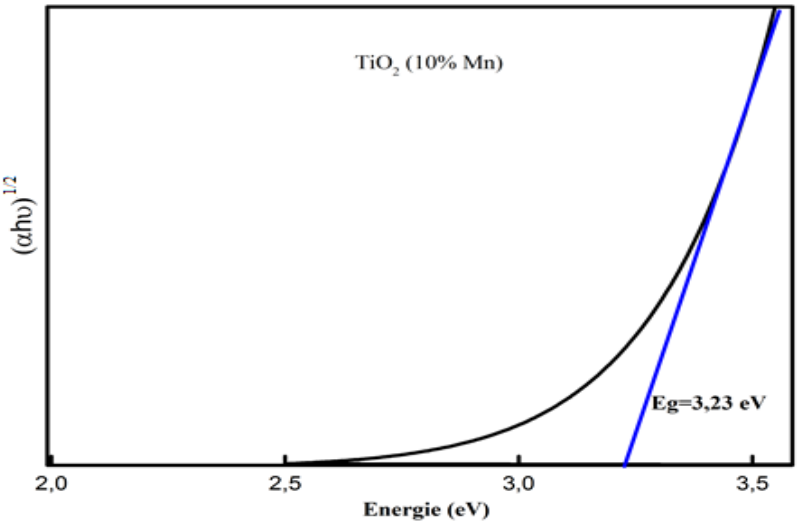

Figure 9. Graphical presentation of the gap energy of Mn doped TiO_2.

Figure 10 shows the variation of the optical gap energy E_g of TiO_2 (Mn) after co-doping with different Cerium fractions. It is observed that the gap energy decreases from 3.23 eV down to 2.97 eV. This

variation is caused by the incorporation of Cerium in TiO_2 lattice. This impurity will create defects by creating intermediate energy levels in the forbidden band of TiO_2 which has led to the reduction of its optical gap (Tbessi *et al.* 2018). These findings are in good agreement with that found by Singh & Mehata, 2019, who developed the mix phase of TiO_2 NPs, at low temperature method at different annealing temperature ranging from 400 to 900 °C, presenting higher efficient for the degradation of dye (RhB) under UV irradiation. Furthermore, the gap energy values obtained correlate well with the Titanium dioxide (TiO_2) photocatalysts in the form of thin films (Zhang and Xu, (2020)). The Eg obtained arranged between 2.28 and 3.25 eV (Sheikhi *et al.* 2019; Kaleji *et al.* 2013; Rangel-Vázquez *et al.* 2015).

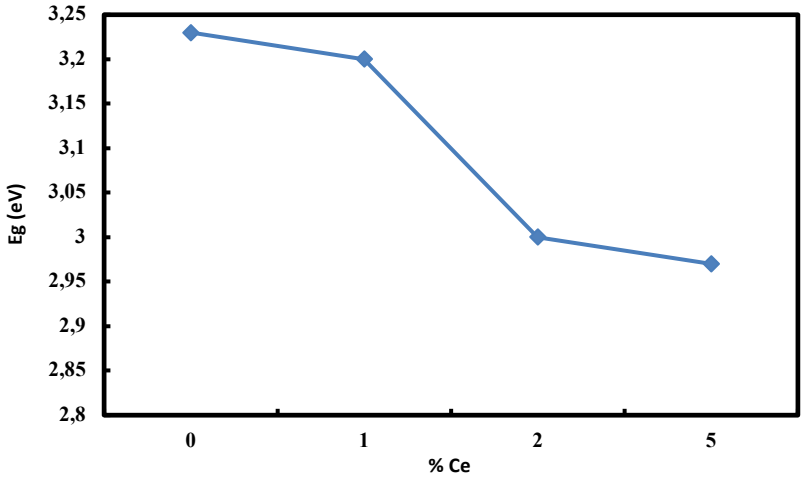

Figure 10. Evolution of the gap energy Eg of Mn-doped TiO_2 after adding Cerium.

Conclusion

Mn-doped and Mn/Ce co-doped TiO_2 nanoparticles have been successfully prepared by a simple precipitation process. The presence of oxygen-titanium bond at 530 cm^{-1} and 629 cm^{-1} confirmed par FTIR spectrum and the presence of the anatse and rutile phases indicated by XRD proved the formation of TiO_2 nanomaterial. The particles size of TiO_2 was estimated by Sherrer and Williamson Hall methods, the average size is around 29 nm for Mn-doped and its decrease to 10 nm for Mn/Ce co-doped TiO_2.This decrease is due to the incorporation of Mn and Ce showed by XRF into the TiO_2 lattice. The absorption band was also improved when Mn and Ce dopants were added. The results in this study reveals that the couple (Ce, Mn) doped TiO_2 enhance the UV absorption and can help to increase the performance of the photovoltaic cells.

Disclosure statement: *Conflict of Interest:* I declare that there are no conflicts of interest.
Compliance with Ethical Standards: This article does not contain any studies involving human or animal subjects.

References

Aguilar P. S., Torres F. F. C. (2019) X-ray diffraction line profile analysis: A microstructural study in polymorphic TiO_2., *Mater. Today. Proc.*13, 420–427. doi: https://doi.org/10.1016/j.matpr.2019.03.175

Al-Amin M., Dey S., Rashid T., Ashaduzzaman Md., Shamsuddin. Sayed. (2016) Solar Assisted Photocatalytic Degradation of Reactive Azo Dyes in Presence of Anatase Titanium Dioxide., *Int. J. Eng. Res. Technol.* 2, 14–21.doi: www.ijlret.com‖ Volume 2 Issue 3‖ March 2016 ‖ PP 14-21

Asep B.D.N., Hanif N.P., Risti R., Suryatno W.S. (2022) Cost Analysis and Economic Evaluation for TiO_2 Synthesis using Sol-Gel Method, *Mor. J. Chem.* 10, 013–021 doi.org/10.48317/IMIST.PRSM/morjchem-v10i1.31721

El Afia Z., Messous M. Y., Cherkaoui M., Tahri M. (2020) Synthesis, Structural and Optical Characterization of Titanium Dioxide Doped by (Ce,Yb) Dedicated to Photonic Conversion., *Indones. J. Chem*. 175–181. doi: 10.22146/ijc.43947

Boxiong S., Ting L., Ning Z., Xiaoyan Y., Lidan D., (2010) Iron-doped Mn-Ce/TiO_2 catalyst for low temperature selective catalytic reduction of NO with NH_3, *J. Environ. Sci*. 22, 1447–1454. https://doi.org/10.1016/S1001-0742(09)60274-6

Cho H W., Liao K L.,Yang J S. (2018) Revelation of rutile phase by Raman scattering for enhanced photo electrochemical performance of hydrothermally-grown anatase TiO_2 film, *Appl. Surf. Sci.* 440 125–132. doi: https://doi.org/10.1016/j.apsusc.2018.01.139

Devi P. O., Milan B P., Han J K., (2020) Investigation of electrochemical performance of a high surface area mesoporous Mn doped TiO_2 nanoparticle for a supercapacitor., *Mater. Lett.* 264, 127363. doi: https://doi.org/10.1016/j.matlet.2020.127363

Ghulam N., Qurat U. A., Tahir M B., Khalid N. R., Tahir I., Muhammad R., Sajad H., Waseem R., Imran A., Muhammad R. (2020) Green synthesis of TiO_2 nanoparticles using lemon peel extract: their optical and photocatalytic properties, *J. Environ. Anal. Chem*. 1032–1038. doi.org/10.1080/24701556.2020.1732419

Hadi N. C. D., Juhana J., Nurul W., Hideto M., Saied R., Mohd H. D. O., Mukhlis A. R., Nurul N. M. J., Nuor S. S., Atikah M. N., Nur H. A. (2022) A Review of Titanium Dioxide (TiO_2)-Based Photocatalyst for Oilfield-Produced Water Treatment, *membranes,*12, 345. https://doi.org/10.3390/membranes12030345

Haque F.Z., Nandanwar R., Singh P. (2017) Evaluating photodegradation properties of anatase and rutile TiO_2 nanoparticles for organic compounds., *Optik*. 128, 191–200. https://doi.org/10.1016/j.ijleo.2016.10.025

Ilie A G., Scarisoareanu M., Morjan I., Elena D., Badiceanu M., Mihailescu I. (2017) Principal Component Analysis of Raman spectra for TiO_2 Nanoparticle Characterization, *Appl. Surf. Sci*. 417, 93–103. doi: https://doi.org/10.1016/j.apsusc.2017.01.193

Junrong L., Youfu Z., Wentao X., He L., Shuai L., Bin W., Kun W. (2020) Red-emitting YAG:Ce, Mn transparent ceramics for warm WLEDs application, *J. Adv. Ceram*. 9(1), 45–54. doi.org/10.1007/s40145-019-0346-0

Kaur R., Singla P., Singh K. (2017) Transition metals (Mn, Ni, Co) doping in TiO_2 nanoparticles and their effect on degradation of diethyl phthalate, *Int. J. Environ. Sci. Technol*., 15, 2359–2368. https://doi.org/10.1007/s13762-017-1573-y

Kanan S., Moyet M. A., Arthur R. B., Patterson H. H. (2020) Recent advances on TiO_2 -based photocatalysts toward the degradation of pesticides and major organic pollutants from water bodies, *Catal. Rev. Sci. Eng.,* 62, 1–65. doi:https://doi.org/10.1080/01614940.2019.1613323

Karishma P., Cristian B., Sylvestre T., Tracy J B. (2020) Chapter Two - Lattice disorders of TiO_2 and their significance in the photocatalytic conversion of CO_2, *Adv. Catal.,* 66, 109–233. https://doi.org/10.1016/bs.acat.2020.09.001

Komaraiah D., Radha E., James J., Kalarikkal N., Sivakumara J., Ramana Reddy M.V., Sayanna R. (2019) Effect of particle size and dopant concentration on the Raman and the photoluminescence spectra of TiO_2: Eu^{3+} nanophosphor thin films, *J. Lumin*., 320–333. https://doi.org/10.1016/j.jlumin.2019.03.050

Li W., Liang R., Hu A., Huang Z., Zhou Y N., (2014) Generation of oxygen vacancies in visible light activated one-dimensional iodine TiO_2 photocatalysts., *RSC Adv*. 70. 36959–36966. doi: https://doi.org/10.1039/C4RA04768K

Liao C., Li Y., Tjong SC. (2020) Visible-Light Active Titanium Dioxide Nanomaterials with Bactericidal Properties., *Nanomaterials*, 10(1), 124. doi: 10.3390/nano10010124

Luiz F. K. P., Lucas C. E., Luis V. A. S. (2021) Deposition of TiO_2 thin Films by Dip-Coating Technique from a Two-Phase Solution Method and Application to Photocatalysis., *Mat. Res*. 24(suppl 1). doi: https://doi.org/10.1590/1980-5373-MR-2021-0007

Milan B P., Changho Y., Han J K. (2020) Synthesis of Conducting Bifunctional Polyaniline@Mn-TiO_2 Nanocomposites for Supercapacitor Electrode and Visible Light Driven Photocatalysis., *Catalysts*. 10(5), 546. doi: https://doi.org/10.3390/catal10050546

Mustapha S., Tijani J. O., Ndamitso M. M., Abdulkareem A. S., Shuaib D. T., Amigun A. T., Abubakar H. L. (2021) Facile synthesis and characterization of TiO_2 nanoparticles: X-ray peak profle analysis using Williamson–Hall and Debye–Scherrer methods, *Int. Nano Lett.* 11, 241–261. https://doi.org/10.1007/s40089-021-00338-w

Nasir M., Bagwasi S., Jiao Y., Chen F., Tian B., Zhang J. (2014) Characterization and activity of the Ce and N co-doped TiO2 prepared through hydrothermal method, *Chemical Engineering Journal,* 236, 388-397, ISSN 1385-8947, https://doi.org/10.1016/j.cej.2013.09.095

Kaleji B. K.; Hosseinabadi N.; Fujishima A. (2013) Enhanced photo-catalytic activity of TiO2 nanostructured thin films under solar light by Sn and Nb co-doping. *J. Sol-Gel Sci. Technol.* 65, 195– 203, DOI: 10.1007/s10971-012-2924-2

Kibasomba P. M., Dhlamini S., Maaza M., Liu C. P, Rashad M. M., Diaa A. R., Mwakikunga B. W. (2018) Strain and grain size of TiO_2 nanoparticles from TEM, Raman spectroscopy and XRD: the revisiting of the Williamson-Hall plot method., *Results Phys*. 628–635. doi:10.1016/j.rinp.2018.03.008

Meddouri M., Hammiche L., Slimi O., Djouadi D., Chelouche A. (2016) Effect of cerium on structural and optical properties of ZnO aerogel synthesized in supercritical methanol., *Mater. Sci. Poland*. 34, 659–664. doi: https://doi.org/10.1515/msp-2016-0082

Rangel-Vázquez I.; Del Angel G.; Bertin V.; González F.; Vázquez-Zavala A.; Arrieta A.; Padilla J.; Barrera A.; Ramos-Ramirez E. (2015) Synthesis and characterization of Sn doped TiO2 photocatalysts: Effect of Sn concentration on the textural properties and on the photocatalytic degradation of 2, 4-dichlorophenoxyacetic acid. *J. Alloys Compd.*, 643, S144– S149

Roman V C., Maria A S., Bärbel K., Tilo B.,Viktor P I., Alexander I T., Kateryna L., Matthias E., Roman A S. (2017) Hybrid biocomposites based on titania nanotubes and ahydroxyapatite coating deposited by RF-magnetron sputtering: Surface topography, structure, and mechanical properties., *Appl. Surf. Sci*. 229–237. doi: https://doi.org/10.1016/j.apsusc.2017.07.199

Salhi R., Deschanvres J. L. (2016) Efficient green and red up-conversion emissions in Er/Yb co-doped TiO_2 nanopowders prepared by hydrothermal-assisted sol-gel process., *J. Lumin*. 176, 250–259. doi: https://doi.org/10.1016/j.jlumin.2016.03.011

Scarisoreanu M., Ilie A., Dutu E., Badoi A., Dumitrache F., Tanasa E., Mihailescu CN., Mihailescu I. (2019) Direct nanocrystallite size investigation in microstrained mixed phase TiO_2 nanoparticles by PCA of Raman spectra., *Appl. Surf. Sci*. 470, 507–519.doi: https://doi.org/10.1016/j.apsusc.2018.11.122

Sharotri N., Sharma D., Sud D. (2019) Experimental and theoretical investigations of Mn-N-co-doped TiO_2 photocatalyst for visible light induced degradation of organic pollutants., *J. Mater. Res. Technol*. 5, 3995–4009. doi: https://doi.org/10.1016/j.jmrt.2019.07.008

Sheikhi M.; Guo W.; Dai Y.; Cui M.; Hoo J.; Guo S.; Xu L.; Liu J.; Ye J. (2019). Mechanism of Improved Luminescence Intensity of Ultraviolet Light Emitting Diodes (UV-LEDs) Under Thermal and Chemical Treatments. *IEEE Photonics J.* 11, 1– 8, DOI: 10.1109/JPHOT.2019.2950049

Singh M.K., Mehata M.S., Phase-dependent optical and photocatalytic performance of synthesized titanium dioxide (TiO2) nanoparticles, *Optik,* 193, 163011, https://doi.org/10.1016/j.ijleo.2019.163011

Siyoung N., Sohyeon S., Hyoyoung L. (2022) A Review of Titanium Dioxide (TiO_2)-Based Photocatalyst for Oilfield-Produced Water Treatment, *Membrane*, *12*(3), 345. doi.org/10.3390/membranes12030345

Susana G.S., Jose A.B., Rafael V., Rodriguez F. (2016) Study of Ce^{3+} to Mn^{2+}energytransfer in highly transmission glasses by time-resolved spectroscopy, *J. Mater. Chem. C*. 1–15. https://doi.org/10.1039/C6TC01408A

Tbessi I., Benito M., Molins E., LIorca J., Touati A., Sayadi S., Wahiba N. (2018) Effect of Ce and Mn co-doping on photocatalytic performance of sol-gel TiO_2, *Solide Stat Science*, 88, 20–28. https://doi.org/10.1016/j.solidstatesciences.2018.12.004

Xiaojun M., Wanru Z., Yin C. (2017) Structure and Photocatalytic Properties of Mn-Doped TiO_2 Loaded on Wood-Based Activated Carbon Fiber Composites., *Materials*. 603. doi: 10.3390/ma10060631.

Winfred M. M., Cecil N. M. O., Martin O. O., Francis B. D. (2016) Energetic, electronic and optical properties of lanthanide doped TiO_2: An ab initio LDA+U study., *J. Solid.State.Chem*.129–137. doi: https://doi.org/10.1016/j.jssc.2016.02.003

Zahid R., Manzoor M., Rafiq A., Ikram M., Nafees M., Butt A R., Hussain S G., Ali S. (2018) Influence of Iron Doping on Structural, Optical and Magnetic Properties of TiO_2., *Nanoparticles. electron mater lett*. 5555–5561.doi: https://doi.org/10.1007/s13391-018-0060-z

Zengping C., Yuri L., Meng G., Fengyun X., Peng W., Yu D., Ping Na. (2016) One-pot synthesis of Mn-doped TiO_2 grown on graphene and the mechanism for removal of Cr(VI) and Cr(III), *J. Hazard. Mater*.188–198. doi: https://doi.org/10.1016/j.jhazmat.2016.02.034

Zhang Y. and Xu X. (2020). Machine Learning Band Gaps of Doped-TiO_2 Photocatalysts from Structural and Morphological Parameters, *ACS Omega*, 5, 25, 15344–15352, doi.org/10.1021/acsomega.0c01438

Zhang R., Zhao J., Yang Y., Lu, Z., Shi W. (2016) Understanding electronic and optical properties of La and Mn co-doped anatase TiO_2, *Comput. Condens. Matter*. 6, 5–17. doi.org/10.1016/j.cocom.2016.03.001

(2023) ; https://revues.imist.ma/index.php/morjchem